

Non-Affine Displacements Below Jamming under Athermal Quasi-Static Compression

Harukuni Ikeda^{1,*} and Koji Hukushima^{1,2,†}

¹*Graduate School of Arts and Sciences, The University of Tokyo 153-8902, Japan*

²*Komaba Institute for Science, The University of Tokyo, 3-8-1 Komaba, Meguro, Tokyo 153-8902, Japan*

(Dated: January 25, 2022)

Critical properties of frictionless spherical particles below jamming are studied using extensive numerical simulations, paying particular attention to the non-affine part of the displacements during the athermal quasi-static compression. It is shown that the squared norm of the non-affine displacement exhibits a power-law divergence toward the jamming transition point. A possible connection between this critical exponent and that of the shear viscosity is discussed. The participation ratio of the displacements vanishes in the thermodynamic limit at the transition point, meaning that the non-affine displacements are localized marginally with a fractal dimension. Furthermore, the distribution of the displacement is shown to have a power-law tail, the exponent of which is related to the fractal dimension.

I. INTRODUCTION

Considering the process of increasing the density of particle system at zero temperature, if the density is low enough, the particles do not overlap. At a certain density, the particles begin to come into contact, and as a result, the system suddenly gains finite energy, mechanical pressure, and stiffness without any apparent structural changes [1]. This phenomenon called jamming has been actively studied in recent years, and the onset is defined as the jamming transition point φ_J . The jamming transition is ubiquitously observed for very diverse athermal systems such as metallic bolls [2], forms [3, 4], colloids [5], polymers [6], candies [7], dices [8], biological tissues [9], growing microbes [10], and some neural networks [11, 12].

A famous and popular numerical protocol to generate a jamming configuration is the athermal quasi-static compression (AQC), which combines the affine transformation with successive energy minimization [13]. An advantage of this protocol is that one can unambiguously define the jamming transition point φ_J as the packing fraction φ at which the energy after the minimization has a non-zero finite value. With the AQC, extensive work has been done for frictionless, spherical, and purely repulsive particles above jamming $\varphi > \varphi_J$. Systematic numerical studies including finite size scaling analyses determine the precise values of the critical exponents in two and three spatial dimensions [13–15], and quasi-one dimension [16]. The numerical results of the critical exponents well agree with the mean-field predictions in two and three dimensions [17, 18].

Contrarily and somewhat surprisingly, the critical properties of the jamming transition below φ_J during the AQC have not yet been fully investigated even for frictionless spherical particles. One of the reasons is that the quantities showing the criticality above φ_J , such as the mechanical pressure, energy, and bulk/shear mod-

ulus, are trivially zero below φ_J , and other appropriate quantities are not necessarily clear below φ_J [13]. The criticality below φ_J has been mainly investigated by adding thermal fluctuation [18, 19], introducing a moving tracer [20], considering self-propelled particles [21], or quenching from random initial configurations [22, 23]. In particular, extensive work has been conducted on shear-driven systems [24–30]. However, it would be more desirable if one can directly extract the criticality from the configurations during the AQC. A promising study in this direction has been done by Shen *et al.* [31]. They observed a rapid increase of several physical quantities, such as the displacements of the particle positions, just below φ_J . However, the critical exponent below φ_J under the AQC has not been calculated yet.

In this work, we characterize the criticality below φ_J during the AQC by investigating the statistical properties of the non-affine displacements for frictionless spherical particles in three dimensions. We show that the mean square of the non-affine displacements diverges toward φ_J with the critical exponent very close to that of the shear viscosity. By observing the participation ratio, it is shown that the displacements become more localized as the system approaches φ_J . Furthermore, by using the finite size scaling of the participation ratio, we calculate the fractal dimension of the displacements at φ_J . Finally, we show that the distribution of the non-affine displacements has a power-law tail at φ_J , and prove that there is a scaling relation between the power-law tail and fractal dimension.

II. MODEL

We consider N frictionless spherical particles in three dimensions. The interaction potential between N particles is given as

$$V = \sum_{i < j}^{1, N} \frac{h_{ij}^2}{2} \theta(-h_{ij}), \quad h_{ij} = |\mathbf{r}_i - \mathbf{r}_j| - R_i - R_j, \quad (1)$$

* hikeda@g.ecc.u-tokyo.ac.jp

† k-hukushima@g.ecc.u-tokyo.ac.jp

where $\mathbf{r}_i = \{x_i, y_i, z_i\}$ and R_i respectively denote the position and radius of the i -th particle. The particles are confined in a cubic box $\mathbf{r}_i \in [0, L]^3$ with the periodic boundary conditions in all directions. To avoid crystallization, we use a binary mixture consisting of $N_S = N/2$ small particles and $N_L = N/2$ large particles. The radii of large and small particles are $R_S = 0.5$ and $R_L = 0.7$, respectively. With those notations, the volume fraction φ is written as

$$\varphi = \frac{2\pi N(R_S^3 + R_L^3)}{3L^3}. \quad (2)$$

The settings of this model are standard ones that have been studied in the context of the jamming transition [13].

III. NUMERICAL SIMULATIONS

Here we describe the AQC originally proposed by O'Hern *et al.* [13]. Starting from a random initial configuration at a small packing fraction, for example $\varphi = 0.1$, compression and energy minimization are performed successively in sequence. For each step of the compression, the packing fraction is slightly increased as $\varphi \rightarrow \varphi + \varepsilon$ with $\varepsilon = 10^{-5}$, by performing the affine transformation $\mathbf{r}_i \rightarrow \mathbf{r}_i L(\varphi + \varepsilon)/L(\varphi)$, where $L(\varphi) = [2\pi N(R_S^3 + R_L^3)/3\varphi]^{1/3}$. Then, the energy is minimized by using the FIRE algorithm, for details see Ref. [32], until the energy or squared force becomes sufficiently small: $V_N/N < 10^{-16}$ or $\sum_{i=1}^N (\nabla_i V_N)^2/N < 10^{-25}$. The procedure is repeated up to the jamming transition point φ_J at which $V_N/N > 10^{-16}$ after the minimization [13].

We perform the numerical simulations for various system sizes $N = 256, 512, 1024, 2048,$ and 4096 . To improve the statistics, we average over 1000 samples for $N = 256$ and 100 samples for the other system sizes. We confirmed that the results do not depend on ε , see Appendix A.

IV. MEAN SQUARED DISPLACEMENT

When the system is compressed from φ to $\varphi + \varepsilon$, the displacement of the i -th particle can be written as

$$\mathbf{r}_i(\varphi + \varepsilon) - \mathbf{r}_i(\varphi) = \delta\mathbf{r}_i^A + \delta\mathbf{r}_i^{\text{NA}} \quad (3)$$

where $\delta\mathbf{r}_i^A = [L(\varphi + \varepsilon)/L(\varphi) - 1]\mathbf{r}_i(\varphi)$ and $\delta\mathbf{r}_i^{\text{NA}}$ respectively denote the affine and non-affine parts of the displacement. In this work, we only focus on the non-trivial part of the displacement $\delta\mathbf{r}_i^{\text{NA}}$.

To characterize the criticality of the non-affine displacements, we first observe the mean squared displacement

$$\langle \Delta \rangle = \frac{1}{N} \sum_{i=1}^N \Delta_i, \quad (4)$$

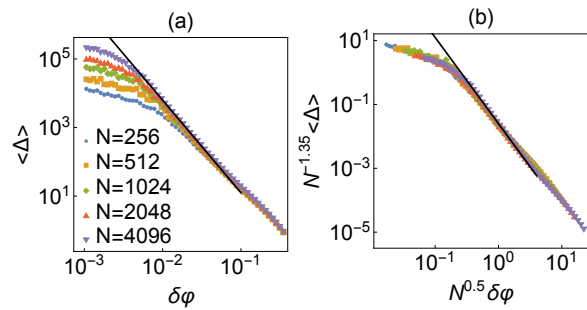


FIG. 1. (a) Mean squared non-affine displacement $\langle \Delta \rangle$. Markers denote numerical results, while the solid line denotes the power law $\Delta \propto \delta\varphi^{-2.7}$. (b) Scaling plot of the same data as in (a).

with

$$\Delta_i = \frac{(\delta\mathbf{r}_i^{\text{NA}})^2}{3\delta l^2}, \quad (5)$$

where $\delta l = L(\varphi + \varepsilon)/L(\varphi) - 1$ accounts for the change of the linear distance L of the system. In Fig. 1 (a), we show $\langle \Delta \rangle$ as a function of $\delta\varphi = \varphi_J - \varphi$. For large N and intermediate $\delta\varphi$, $\langle \Delta \rangle$ shows the power law

$$\langle \Delta \rangle \propto \delta\varphi^{-\beta}. \quad (6)$$

The power-law fitting of the data for $N = 4096$ in the range $\delta\varphi \in (0.01, 0.1)$ leads to

$$\beta = 2.7, \quad (7)$$

see the solid line in Fig. 1 (a). Interestingly, Eq. (7) is close to the theoretical prediction for the critical exponent of the shear viscosity $\beta' = 2.8$ [33]. We shall discuss a possible connection between $\langle \Delta \rangle$ and shear viscosity later in this paper.

To further investigate the scaling of $\langle \Delta \rangle$, we perform a finite-size scaling analysis assuming the following scaling function:

$$\langle \Delta \rangle = N^\alpha \mathcal{D}(N^{\alpha/\beta} \delta\varphi), \quad (8)$$

where $\mathcal{D}(x) = O(1)$ for $x \ll 1$, and $\mathcal{D}(x) \sim x^{-\beta}$ for $x \gg 1$. As shown in Fig. 1 (b), a good scaling collapse is obtained with $\alpha = 1.35$. This result implies that the number of the correlated particles diverges as $N_{\text{cor}} \sim \delta\varphi^{-\beta/\alpha} \sim \delta\varphi^{-2}$, and the correlation length $L_{\text{cor}} \sim N_{\text{cor}}^{1/3} \sim \delta\varphi^{-\nu}$ with $\nu = 2/3 \approx 0.67$ under the assumption that the correlated volume is compact. This is close to a previous result $\nu = 0.71$ obtained by the finite-size scaling analysis of the transition point [13].

V. PARTICIPATION RATIO

To see the spatial structure of the displacements, we observe the normalized vector [34]:

$$\mathbf{e}_i = \frac{\delta \mathbf{r}_i^{\text{NA}}}{\sqrt{\sum_{i=1}^N (\delta \mathbf{r}_i^{\text{NA}})^2}}, \quad (9)$$

which satisfies $\sum_{i=1}^N \mathbf{e}_i \cdot \mathbf{e}_i = 1$. In Fig. 2, we visualize \mathbf{e}_i by drawing spheres such that their radii are proportional to $|\mathbf{e}_i|$. Far from jamming, the spatial distribution of \mathbf{e}_i is homogeneous and featureless, see Fig. 2 (a). On the contrary, near jamming, a few particles have very large displacements, and thus the displacement is spatially heterogeneous and localized, see Fig. 2 (d). We quantify the degree of the localization by using the participation ratio:

$$P = \frac{1}{N} \frac{\left(\sum_{i=1}^N \mathbf{e}_i \cdot \mathbf{e}_i\right)^2}{\sum_{i=1}^N (\mathbf{e}_i \cdot \mathbf{e}_i)^2}, \quad (10)$$

which (or inverse of which) is widely used in the study of condensed matter physics [35], including amorphous solids [36, 37]. If \mathbf{e}_i is spatially localized to a single particle, say $\mathbf{e}_i \cdot \mathbf{e}_i = \delta_{i1}$, the participation ratio P is proportional to N^{-1} . On the contrary, if \mathbf{e}_i is extended such that $\mathbf{e}_i \cdot \mathbf{e}_i \sim N^{-1}$ for all i , P is constant independent of N . In Fig. 3 (a), we show the $\delta\varphi$ dependence of P . One can see that P decreases with approaching φ_J and increasing N . To investigate the N dependence of P , we use the following scaling form:

$$P = N^{-\gamma} \mathcal{P}(N^{\alpha/\beta} \delta\varphi), \quad (11)$$

assuming the same correlated volume as in Eq. (8). We find a good collapse with

$$\gamma = 0.32 \quad (12)$$

near the jamming point, see Fig. 3 (b). At φ_J , P vanishes in the thermodynamic limit as $P \sim N^{-\gamma}$. This exponent relates to the fractal dimension d_f of \mathbf{e}_i , namely, if $\mathbf{e}_i \cdot \mathbf{e}_i \sim L^{-d_f}$ for $i = 1, \dots, L^{d_f}$, this yields that $P \sim N^{-1+d_f/d}$ [35], leading to

$$d_f = 3(1 - \gamma) = 2.04. \quad (13)$$

Therefore, \mathbf{e}_i has a more compact structure than the bulk $d = 3$. A mean-field theory of the jamming transition predicts that the correlated volume v_{col} and correlation length l_{cor} have the following relation $v_{\text{col}} \sim l_{\text{cor}}^2$ [38, 39]. This may imply that the fractal dimension is $d_f = 2$, which is close to our estimation Eq. (13).

Interestingly, the similar spatially heterogeneous structures are observed for super-cooled liquids near the glass transition point [40]. For the studies of the glass transition, the degree of spatial heterogeneity is characterized

by the so-called non-gaussian parameter [41, 42]. In our setting, an analogous quantity may be written as

$$\alpha_2 = \frac{3 \langle (\delta \mathbf{r}^{\text{NA}})^4 \rangle}{5 \langle (\delta \mathbf{r}^{\text{NA}})^2 \rangle^2} - 1 = \frac{3}{5P} - 1. \quad (14)$$

If the displacements follow the featureless gaussian distribution, one obtains $\alpha_2 = 0$. For the supercooled liquids, α_2 of the displacements rapidly increases on decreasing the temperature [42, 43]. Similarly, α_2 of our model increases on approaching φ_J , because $P \rightarrow 0$ and $\alpha_2 \propto P^{-1}$. Furthermore, an experimental study for the supercooled colloidal suspensions, which approximately behave as hard spheres [44, 45] and may have the same interaction as our model below jamming, showed that the dynamically correlated regions form a compact cluster of the fractal dimension $d_f = 1.9 \pm 0.4$ [43], reasonably close to our result of Eq. (13). Also, the inhomogeneous mode-coupling theory, which is a mean-field theory of the glass transition, predicts $d_f = 2$ in the early stage of the relaxation process [46]. Those results suggest the existence of the underlying universality between the dynamics of the athermal system near φ_J and thermal systems near the glass transition point [47, 48].

VI. DISTRIBUTION FUNCTION

Here, we discuss the behavior of P from the perspective of the distribution of Δ . First, we note that P can be written as

$$P = \frac{[\int_0^\infty d\Delta f(\Delta) \Delta]^2}{\int_0^\infty d\Delta f(\Delta) \Delta^2}, \quad (15)$$

where the distribution $f(\Delta)$ of Δ is defined as

$$f(\Delta) = \frac{1}{N} \sum_{i=1}^N \delta(\Delta - \Delta_i). \quad (16)$$

Fig. 4 (a) presents $f(\Delta)$ for several $\delta\varphi$. $f(\Delta)$ has a broader distribution for smaller $\delta\varphi$. For the later convenience, we define a scaled variable $x = \Delta / \langle \Delta \rangle$, and distribution function

$$\mathcal{F}(x) = f(\Delta) \frac{d\Delta}{dx} = \langle \Delta \rangle f(\langle \Delta \rangle x). \quad (17)$$

By definition, $\int dx \mathcal{F}(x) = \int dx f(x) x = 1$. As shown in Fig. 4 (b), with decreasing $\delta\varphi$, $\mathcal{F}(x)$ develops the power-law tail

$$\lim_{\delta\varphi \rightarrow 0} \mathcal{F}(x) \sim x^{-\zeta} \text{ for } x \gg 1. \quad (18)$$

A similar fat-tail was previously reported for the velocity distribution of sheared driven systems in the quasi-static limit near φ_J [49–51]. Now, we show that the exponent

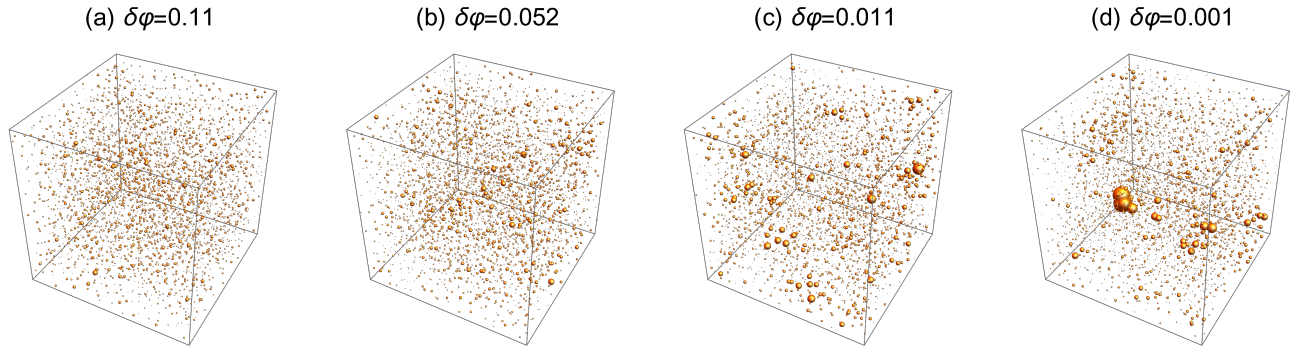


FIG. 2. Spatial distribution of non-affine displacements for $N = 4092$ particles. Diameters of spheres represent the amplitude of the (normalized) non-affine displacements $|e_i|$.

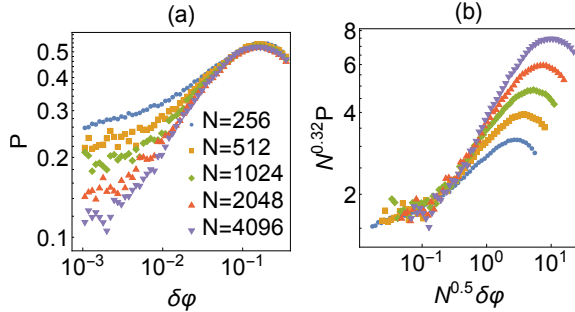


FIG. 3. (a) Participation ratio P . Markers denote numerical results. (b) Scaling plot of the same data.

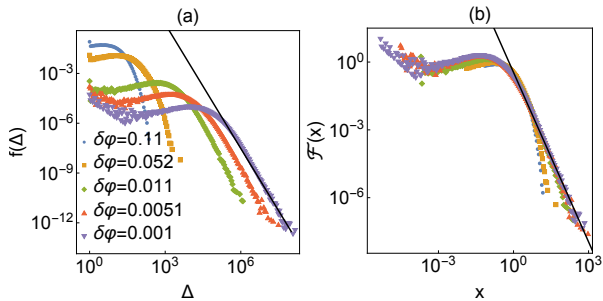


FIG. 4. (a) Distribution of Δ for $N = 4096$. Markers are numerical results, while the solid line denotes the power law $f(\Delta) \sim \Delta^{-2.5}$. (b) Distribution of $x = \Delta / \langle \Delta \rangle$ for the same data. The solid line denotes $\mathcal{F}(x) \sim x^{-2.5}$.

ζ relates to γ in Eq. (11). Using Eq. (15) and (17), we get

$$P = \left(\int_0^\infty dx x^2 \mathcal{F}(x) \right)^{-1}. \quad (19)$$

If $\zeta < 3$, the denominator diverges, leading to $P = 0$ at φ_J . For finite N , however, the divergence does not occur as the power law of $\mathcal{F}(x)$ is truncated at finite x_{\max} . Using the extreme value statistics, we can calculate x_{\max} as

$$\int_{x_{\max}}^\infty \mathcal{F}(x) dx \sim \frac{1}{N} \rightarrow x_{\max} \sim N^{\frac{1}{\zeta-1}}. \quad (20)$$

Then, P for finite N is expressed as

$$P \sim \left(\int_0^{x_{\max}} dx x^2 \mathcal{F}(x) \right)^{-1} \sim N^{-\frac{3-\zeta}{\zeta-1}}. \quad (21)$$

Comparing this with Eq. (11) for $\delta\varphi = 0$, we finally get

$$\zeta = \frac{3 + \gamma}{1 + \gamma} = 2.5. \quad (22)$$

This is consistent with the assumption $\zeta < 3$ and well agrees with the numerical result, see Fig. 4.

VII. SUMMARY AND DISCUSSIONS

In summary, we investigated the statistical properties of the non-affine displacements under the AQC below the jamming transition point. We showed that the mean square of the non-affine displacement diverges toward the jamming transition point. At the jamming transition point, the distribution of the non-affine displacements has a power-law tail, the exponent of which relates to the fractal dimension.

An interesting question is how the present work relates to the previous works for the shear driven systems. As the shear viscosity η diverges with the same critical exponent as the bulk viscosity η_p near φ_J , namely, $\eta \sim \eta_p \sim \delta\varphi^{-\beta'}$ [52, 53], we consider a system compressed with a finite compression rate $\dot{l} = \dot{L}/L$, instead of the shear driven system. The work done by the imposed compression per time is $p\dot{l}L^3 = \eta_p \dot{l}^2 L^3$, where p denotes

the pressure, and $\eta_p = p/\dot{l}$ denotes the bulk viscosity. In the quasi-static limit $\dot{l} \rightarrow 0$, this should be balanced with the dissipation $\sum_{i=1}^N (\dot{\mathbf{r}}_i^{\text{NA}})^2$, leading to [28, 54]

$$\eta_p \sim \frac{1}{L^3} \sum_{i=1}^N \left(\frac{\dot{\mathbf{r}}_i^{\text{NA}}}{l} \right)^2 \sim \frac{1}{L^3} \sum_{i=1}^N \left(\frac{\delta \mathbf{r}_i^{\text{NA}}}{\delta l} \right)^2 \sim \langle \Delta \rangle. \quad (23)$$

A mean-field theory of sheared suspensions predicts $\eta \sim \delta\varphi^{-\beta'}$ with $\beta' = 2.8$ [33], which is close to our result $\langle \Delta \rangle \sim \delta\varphi^{-\beta}$ with $\beta = 2.7$ and thus supports the above conjecture. However, the numerical result of β' varies widely from one literature to another. For instance, Ref. [29] reported $\beta' = 2.55$, while Ref. [30] reported $\beta' = 3.82$. Further study is necessary to elucidate this point.

From a practical point of view, the AQC has several advantages over other dynamical methods such as implying shear to characterize the criticality below jamming. First of all, our method is much efficient, as we do not need to wait that the system reaches the steady state. Furthermore, the method allows us to reduce the fitting parameters because the jamming transition point φ_J is determined during the procedure. Therefore, we believe that the AQC facilitates the investigation of the criticality below jamming for frictionless spherical particles, and hopefully for other models such as non-spherical particles and frictional particles. For frictional particles, it is reported that the waiting time and its distribution show the power-law behaviors near the (shear) jamming transition point [55, 56]. It is an interesting future work to see if such critical behaviors of the dynamical quantities appear under the AQC protocol.

The mean-field theory predicts that the correlated volume has the fractal dimension $d_f = 2$, irrespective of the spatial dimension d [38, 39]. If this is the case, the similar argument above Eq. (13) leads to

$$\gamma = \frac{d-2}{d}, \quad (24)$$

and that of Eq. (22) leads to

$$\zeta = \frac{2d-1}{d-1}. \quad (25)$$

We obtained numerical results consistent with Eqs. (24) and (25) in three dimension $d = 3$. It is tempting to test if Eqs. (24) and (25) hold in other d . In particular, $\gamma = 0$ in $d = 2$, suggesting that the participation ratio P at φ_J may exhibit the logarithmic dependence on N , instead of a power law. This deserves further study.

ACKNOWLEDGMENTS

We warmly thank A. Ikeda for discussions related to this work. We also thank S. Teitel and anonymous referees for useful comments. This project has received funding from the JSPS KAKENHI Grant Number JP20J00289.

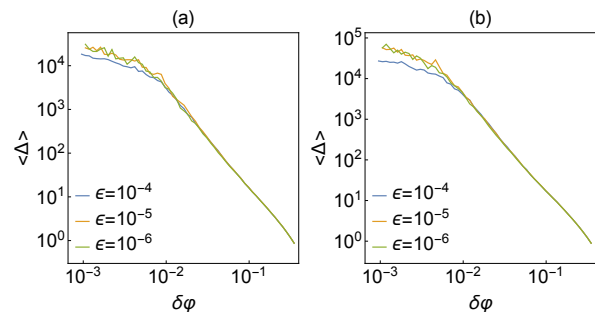


FIG. 5. $\delta\varphi$ dependence of $\langle \Delta \rangle$ with varying ϵ for $N = 512$ (a) and $N = 1024$ (b).

Appendix A: ϵ dependence

Here we show numerical results of examining the ϵ dependence in our simulation protocol. Fig. 5 presents the ϵ dependence of $\langle \Delta \rangle$ for $N = 512$ and $N = 1024$. One can see that the results do not depend on ϵ for $\epsilon \leq 10^{-5}$. The similar ϵ dependencies of the physical quantities have been previously reported by the numerical study of the quasi-static shear [57]. Therefore, in this study, our simulation was performed with $\epsilon = 10^{-5}$.

[1] M. Van Hecke, *J. Phys. Condens. Matter* **22**, 033101 (2009).
 [2] J. Bernal and J. Mason, *Nature* **188**, 910 (1960).
 [3] D. J. Durian, *Phys. Rev. Lett.* **75**, 4780 (1995).
 [4] G. Katgert and M. van Hecke, *EPL* **92**, 34002 (2010).
 [5] Z. Zhang, N. Xu, D. T. Chen, P. Yunker, A. M. Alsayed, K. B. Aptowicz, P. Habdas, A. J. Liu, S. R. Nagel, and A. G. Yodh, *Nature* **459**, 230 (2009).

[6] N. C. Karayiannis, K. Foteinopoulou, and M. Laso, *J. Chem. Phys.* **130**, 164908 (2009).
 [7] A. Donev, I. Cisse, D. Sachs, E. A. Variano, F. H. Stillinger, R. Connelly, S. Torquato, and P. M. Chaikin, *Science* **303**, 990 (2004).
 [8] A. Jaoshvili, A. Esakia, M. Porrati, and P. M. Chaikin, *Phys. Rev. Lett.* **104**, 185501 (2010).
 [9] D. Bi, J. Lopez, J. Schwarz, and M. L. Manning, *Nat. Phys.* **11**, 1074 (2015).

- [10] M. Delarue, J. Hartung, C. Schreck, P. Gniewek, L. Hu, S. Herminghaus, and O. Hallatschek, *Nat. Phys.* **12**, 762 (2016).
- [11] S. Franz and G. Parisi, *J. Phys. A* **49**, 145001 (2016).
- [12] S. Franz, S. Hwang, and P. Urbani, *Phys. Rev. Lett.* **123**, 160602 (2019).
- [13] C. S. O'Hern, L. E. Silbert, A. J. Liu, and S. R. Nagel, *Phys. Rev. E* **68**, 011306 (2003).
- [14] C. P. Goodrich, A. J. Liu, and S. R. Nagel, *Phys. Rev. Lett.* **109**, 095704 (2012).
- [15] P. Charbonneau, E. I. Corwin, G. Parisi, and F. Zamponi, *Phys. Rev. Lett.* **114**, 125504 (2015).
- [16] H. Ikeda, *Phys. Rev. Lett.* **125**, 038001 (2020).
- [17] M. Wyart, L. E. Silbert, S. R. Nagel, and T. A. Witten, *Phys. Rev. E* **72**, 051306 (2005).
- [18] P. Charbonneau, J. Kurchan, G. Parisi, P. Urbani, and F. Zamponi, *Nat. Commun.* **5**, 1 (2014).
- [19] A. Ikeda, L. Berthier, and G. Biroli, *J. Chem. Phys.* **138**, 12A507 (2013).
- [20] J. A. Drocco, M. B. Hastings, C. J. O. Reichhardt, and C. Reichhardt, *Phys. Rev. Lett.* **95**, 088001 (2005).
- [21] Q. Liao and N. Xu, *Soft Matter* **14**, 853 (2018).
- [22] A. Ikeda, T. Kawasaki, L. Berthier, K. Saitoh, and T. Hatano, *Phys. Rev. Lett.* **124**, 058001 (2020).
- [23] Y. Nishikawa, A. Ikeda, and L. Berthier, *arXiv preprint arXiv:2007.09418* (2020).
- [24] G. Marty and O. Dauchot, *Phys. Rev. Lett.* **94**, 015701 (2005).
- [25] P. Olsson and S. Teitel, *Phys. Rev. Lett.* **99**, 178001 (2007).
- [26] T. Hatano, *J. Phys. Soc. Jpn.* **77**, 123002 (2008).
- [27] C. Heussinger and J.-L. Barrat, *Phys. Rev. Lett.* **102**, 218303 (2009).
- [28] E. Lerner, G. Düring, and M. Wyart, *PNAS* **109**, 4798 (2012).
- [29] T. Kawasaki, D. Coslovich, A. Ikeda, and L. Berthier, *Phys. Rev. E* **91**, 012203 (2015).
- [30] P. Olsson, *Phys. Rev. Lett.* **122**, 108003 (2019).
- [31] T. Shen, C. S. O'Hern, and M. D. Shattuck, *Phys. Rev. E* **85**, 011308 (2012).
- [32] E. Bitzek, P. Koskinen, F. Gähler, M. Moseler, and P. Gumbsch, *Phys. Rev. Lett.* **97**, 170201 (2006).
- [33] E. DeGiuli, G. Düring, E. Lerner, and M. Wyart, *Phys. Rev. E* **91**, 062206 (2015).
- [34] R. Yamamoto and A. Onuki, *Phys. Rev. Lett.* **81**, 4915 (1998).
- [35] B. Kramer and A. MacKinnon, *Rep. Prog. Phys.* **56**, 1469 (1993).
- [36] E. Lerner, G. Düring, and E. Bouchbinder, *Phys. Rev. Lett.* **117**, 035501 (2016).
- [37] H. Mizuno, H. Shiba, and A. Ikeda, *PNAS* **114**, E9767 (2017).
- [38] L. Yan, E. DeGiuli, and M. Wyart, *EPL* **114**, 26003 (2016).
- [39] G. Düring, E. Lerner, and M. Wyart, *Phys. Rev. E* **94**, 022601 (2016).
- [40] M. D. Ediger, *Annu. Rev. Phys. Chem.* **51**, 99 (2000).
- [41] A. Rahman, *Phys. Rev.* **136**, A405 (1964).
- [42] W. Kob and H. C. Andersen, *Phys. Rev. E* **51**, 4626 (1995).
- [43] E. R. Weeks, J. C. Crocker, A. C. Levitt, A. Schofield, and D. A. Weitz, *Science* **287**, 627 (2000).
- [44] P. N. Pusey and W. Van Meegen, *Nature* **320**, 340 (1986).
- [45] W. van Meegen and S. M. Underwood, *Phys. Rev. E* **49**, 4206 (1994).
- [46] G. Biroli, J.-P. Bouchaud, K. Miyazaki, and D. R. Reichman, *Phys. Rev. Lett.* **97**, 195701 (2006).
- [47] G. Marty and O. Dauchot, *Phys. Rev. Lett.* **94**, 015701 (2005).
- [48] P. Chaudhuri, L. Berthier, and W. Kob, *Phys. Rev. Lett.* **99**, 060604 (2007).
- [49] B. P. Tighe, E. Woldhuis, J. J. C. Remmers, W. van Saarloos, and M. van Hecke, *Phys. Rev. Lett.* **105**, 088303 (2010).
- [50] B. Andreotti, J.-L. Barrat, and C. Heussinger, *Phys. Rev. Lett.* **109**, 105901 (2012).
- [51] P. Olsson, *Phys. Rev. E* **93**, 042614 (2016).
- [52] P. Olsson and S. Teitel, *Phys. Rev. Lett.* **109**, 108001 (2012).
- [53] D. Vågberg, P. Olsson, and S. Teitel, *Phys. Rev. Lett.* **113**, 148002 (2014).
- [54] G. Katgert, B. P. Tighe, and M. van Hecke, *Soft Matter* **9**, 9739 (2013).
- [55] R. Pastore, M. P. Ciamarra, and A. Coniglio, *Philosophical Magazine* **91**, 2006 (2011).
- [56] I. Srivastava, L. E. Silbert, G. S. Grest, and J. B. Lechman, *Phys. Rev. Lett.* **122**, 048003 (2019).
- [57] D. Vågberg, P. Olsson, and S. Teitel, *Phys. Rev. E* **83**, 031307 (2011).